Temperature dependent Raman scattering and far-infrared reflectance spectra of MgO modified Pb0.99(Zr0.95Ti0.05)0.98Nb0.02O3 ceramics: A composition effect

Z. H. Duan, P. Chang, Z. G. Hu, J. X. Wang, G. S. Wang, X. L. Dong, and J. H. Chu

Citation: Journal of Applied Physics **116**, 093513 (2014); doi: 10.1063/1.4894467
View online: http://dx.doi.org/10.1063/1.4894467
View Table of Contents: http://scitation.aip.org/content/aip/journal/jap/116/9?ver=pdfcov
Published by the AIP Publishing

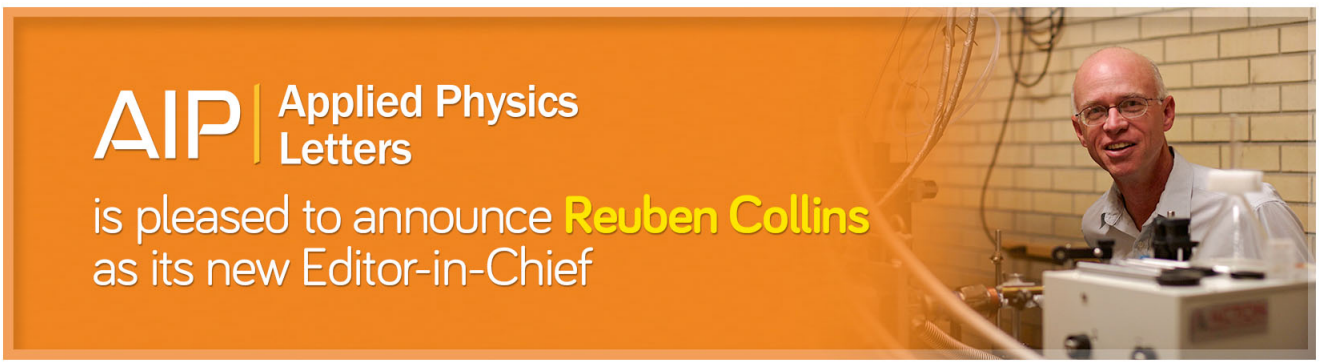

Temperature dependent Raman scattering and far-infrared reflectance spectra of MgO modified $Pb_{0.99}(Zr_{0.95}Ti_{0.05})_{0.98}Nb_{0.02}O_3$ ceramics: A composition effect

Z. H. Duan (段志华),[1] P. Chang (常平),[1] Z. G. Hu (胡志高),[1,a)] J. X. Wang (王军霞),[2] G. S. Wang (王根水),[2] X. L. Dong (董显林),[2] and J. H. Chu (褚君浩)[1]
[1]*Key Laboratory of Polar Materials and Devices, Ministry of Education, Department of Electronic Engineering, East China Normal University, Shanghai 200241, China*
[2]*Key Laboratory of Inorganic Functional Materials and Devices, Shanghai Institute of Ceramics, Chinese Academy of Sciences, Shanghai 200050, China*

(Received 17 July 2014; accepted 21 August 2014; published online 4 September 2014)

Lattice dynamics and phase transition of MgO modified $Pb_{0.99}(Zr_{0.95}Ti_{0.05})_{0.98}Nb_{0.02}O_3$ (PZTN-x wt. % MgO, $x = 0$, 0.1, 0.2, 0.5) ceramics have been investigated by far-infrared (FIR) reflectance in the temperature range of 5.5–300 K and Raman spectra between 77 and 300 K, respectively. With the aid of above complementary methods, the structure of all ceramics was defined as low-temperature ferroelectric rhombohedral phase [$F_{R(LT)}$] at room temperature. The FIR dielectric functions were extracted from the multi-Lorentz oscillator dispersion model. The lowest frequency phonon mode, which is related to Pb-BO_3 (B = Zr, Ti, Nb) vibration, mainly dominates the FIR dielectric response. With increasing MgO composition, the dielectric constants $\varepsilon(0)$ at room temperature are estimated to 85.4, 73.4, 73.9, and 41.9, respectively. The decreasing trend can be due to the doubly ionized oxygen vacancies induced by Mg substitution for B-site. The order-disorder phase transition located around 120 K can be clearly clarified from temperature evolution of phonon frequency, damping, and intensity. It decreases slightly with increasing MgO composition, which influence the distortion due to the broken correlation chains and local permanent dipoles creation. Moreover, the transformation from antiferroelectric orthorhombic A_O to [$F_{R(LT)}$] phase has been observed around 250 K, which is associated with the antiferroelectric displacement of Pb atoms along ⟨110⟩ and coupled rotations of the corner-connected oxygen octahedral. Furthermore, the transition from [$F_{R(LT)}$] to [$F_{R(HT)}$] (high-temperature ferroelectric rhombohedral phase) was identified around 290 K for MgO-doped PZTN ceramics. It arises from the shift of cation (Pb and Zr/Ti/Nb/Mg ions) along the ⟨111⟩ direction and the transition temperature slightly decreases compared to the pure ceramic. © *2014 AIP Publishing LLC*. [http://dx.doi.org/10.1063/1.4894467]

I. INTRODUCTION

Lead zirconate titanate ferroelectric $PbZr_{1-x}Ti_xO_3$ (PZT) is an example of perovskite solid solutions because of the widespread use in piezoelectric transducers and actuators. It is among the best study since the exceptional optical and dielectric properties were revealed and the phase diagram is established.[1] When the composition is located on Zr-rich side (the Zr/Ti ratio close to 95/5), a ferroelectric (FE) and antiferroelectric (AFE) phase boundary is encountered. It can be characterized by the cations adopting an antiparallel arrangement along $[110]_p/[\bar{1}\bar{1}0]_p$ directions in the AFE phase, which is coupled to antiphase rotations of the octahedral around $[110]_p$ axis ($a^-a^-c^0$ tilt system).[2] It separates orthorhombic AFE (A_O) from high- and low-temperature rhombohedral FE phase with symmetry $R3m$ [$F_{R(HT)}$] and $R3c$ [$F_{R(LT)}$], respectively.[3–5] Under the complex physical phenomena, the availability to induce phase transitions by temperature, electric field, and hydrostatic pressure leads to technological applications based on piezoelectric and ferroelectric properties.[3,6]

Furthermore, the physical properties can be substantially improved by substitution of a small amount of isovalent or heterovalent elements for Pb or Zr/Ti sublattices. For example, the La^{3+} ions and accompanying vacancies are distributed on the Pb^{2+} sites, which represent a type of disorder and significantly modify the properties near ferroelectric-relaxor boundary.[7] Below Curie temperature, the phonons also show anomalies around 200 K due to another phase transition to a ferroelectric state with double unit cell.[8] The B-cation arrangement plays an important role in an interplay of bonding, electrostatic, and short-range repulsive interactions, which governs the distortions of the structure away from ideal perovskite structure (ABO_3).[9] The B-site donor (niobium, tantalum, and tungsten) in PZT will increase the oxygen vacancy formation energy and decrease occupied Ti $3d$ states, which can contribute to high fatigue resistance.[10] Among them, niobium (Nb) is widely employed, which substitute Zr^{4+} or Ti^{4+}. The pressure-temperature phase diagram for [$Pb_{0.99}(Zr_{0.95}Ti_{0.05})_{0.98}Nb_{0.02}O_3$, PZTN] has been reported by Fritz and Keck in 1970s.[11,12] Addition with small amount of Nb to this solution can stabilize the $F_{R(LT)}$

a)Author to whom correspondence should be addressed. Electronic mail: zghu@ee.ecnu.edu.cn. Tel.: +86-21-54345150. Fax: +86-21-54345119.

at ambient conditions, reduce aging effects and dielectric loss, and improve resistivity and ferroelectric properties.[3] On the other hand, the application of Nb_2O_5 enlarges the rhombohedral ferroelectric region with respect to that in the pure system, which means that the Jaffe's phase diagram moves on to lower composition as the dopant increases.[1,13] The antiferroelectric transition in Nb-doped PZT 95/5 has extremely large thermal hysteresis and slow kinetics due to the charged defects.[3,14,15] The Mg^{2+} ions, which have lower valency and ionic size, act as acceptor doping and substitute $(Zr,Ti)^{4+}$. It can restrict the domain motion, thereby increasing the cohesive field but reducing the dielectric constant, which is the characteristic property for hard PZTs. Recently, Sanjoom and Puchmark reported that MgO nanoparticles can improve the dielectric behavior and microhardness of PZT ceramics.[16] Especially, (Mg, Nb) co-doping strongly reduces both conductivity levels and the dominant conducting oxygen vacancies.[17] However, few studies about the co-doping and temperature influence on the phonon dispersion and dielectric behavior in far-infrared (FIR) region have been presented.

Phonon dispersion behavior is closely related to the structure symmetry and allows to identify the phase transitions.[18] The study of optical phonons can also provide direct information on even subtle structural distortions. As we know, Raman scatter information is collected through the interaction between laser light and phonon, molecular vibration, or other excitations. The incident infrared (IR) radiation directly couples to the polarization, enabling one to extract the parameters of polar-phonon modes. Both IR and Raman spectroscopy are sensitive to nanoscopic order and powerful in investigating structural and phonon behavior of oxide materials with perovskite structure.[19] For instance, IR and Raman spectra of ferroelectric ceramic and single crystal [PZT, $Pb(Zn_{1/3}Nb_{2/3})O_3$-$PbTiO_3$ etc.] near morphotropic phase boundary (MPB) have been studied to define the local and macroscopic symmetries divergence and identify the boundaries among rhombohedral, monoclinic, and tetragonal phases.[20–23] The dominant local ordering, double occupancy of B-site atoms, and octahedra tilting were clearly analyzed through IR and Raman active modes. In this article, the lattice dynamics of MgO-modified PZNT, dielectric functions, and temperature dependence of phonon mode have been investigated by Raman scattering and FIR reflectance spectra. The phase transition is discovered and discussed on the basis of variations about frequencies, damping, and strength of phonon mode with temperature.

II. EXPERIMENTAL DETAILS

The general chemical formula for the investigated ceramics was $Pb_{0.99}(Zr_{0.95}Ti_{0.05})_{0.98}Nb_{0.02}O_3$–$x$ wt. % MgO, where $x = 0.0$, 0.1, 0.2, and 0.5. The samples were prepared using the traditional solid-state ceramic processing route by mixing PZTN powders with MgO particles. PZTN powders were synthesized from appropriate quantities of high-purity oxide powders (Pb_3O_4, ZrO_2, TiO_2, and Nb_2O_5) by conventional mixed oxide method. Then, the as-prepared sample is processed into disk with a diameter of 12.5 mm and a thickness of about 3 mm. All the wafers were single-side polished, rigorously cleaned in pure ethanol with an ultrasonic bath and rinsed several times by deionized water for spectral measurements.

The phase and crystal structure of PZTN-x wt. % MgO ceramics were determined by X-ray diffraction (XRD) using Cu $K\alpha$ radiation (D/MAX-2550 V, Rigaku Co.). At room temperature (RT), the ceramics are of perovskite structure with ferroelectric rhombohedral phase (not shown). Variable-temperature FIR reflectance spectra were recorded by a Bruker VERTEX 80 V FTIR spectrometer equipped with a specular reflectance setup from 5.5 to 300 K. The globar lamp, 6-μm Mylar beamspitter, and DLaTGS detector were used during the measurements. The ceramics were mounted into an Oxford AC-V12w continuous flow cryostat with the sample in He vapor. Gold mirror, whose absolute reflectance was measured, was taken as reference for the spectra at the corresponding temperatures. On the other hand, temperature-dependent Raman scattering measurements were carried out by a Jobin-Yvon LabRAM HR UV micro-Raman spectrometer. The He-Ne laser with the wavelength of 632.8 nm is taken as the exciting source. The temperature from 77 to 300 K was controlled by a Linkam THMSE 600 heating/cooling stage with a precision of about 0.5 K.

III. RESULTS AND DISCUSSION

A. Infrared reflectance and Raman scattering spectra

Figs. 1(a) and 1(b) present Raman spectra for PZTN ceramic at 77 and 300 K, respectively. The spectra show similar characteristic peaks at 77 K. The bands can be divided into four parts by the dotted lines and classification assigned:[24,25] "I" (below 140 cm^{-1}) is assigned to Pb-(BO_3) (B = Zr, Ti, Nb) vibration modes; "II" (140–248 cm^{-1}) corresponds to O-Zr-O bending modes; "III" (260–400 cm^{-1}) is related to ZrO_3 torsional modes; and "IV" (beyond 500 cm^{-1}) is assigned to Zr-O stretching motions. According to the group theoretical analysis, there exist 12 Raman and 11 IR active modes in the orthorhombic C_{2v} symmetry.[24] As shown in Fig. 1(c), Raman spectra are fitted with the multi-Lorentz peak lineshapes to extract the phonon frequency and the additional modes might be connected with the different atoms on B-site.[23] At ambient condition, the resonant frequency of phonon mode (A symmetry) in the range of 120–150 cm^{-1} (125 and 141 cm^{-1}) is close to twice the frequency of antiferrodistortive motion (63 cm^{-1}). It is similar to the existence of Fermi resonance in $Pb(Zr_{0.48}Ti_{0.52})O_3$ ceramic.[26] It was found that the peaks shift slightly towards a lower wavenumber side with increasing MgO composition, which shows the effect from substitution Zr(Ti) for Mg. In the present case, the ionic radii for PZTN ceramics have been reported as following: $Pb^{2+}[12] = 1.49$, $Zr^{4+}[6] = 0.72$, $Ti^{4+}[6] = 0.605$, $Nb^{5+}[6] = 0.64$, $Mg^{2+}[6] = 0.72$ Å, respectively.[27] The substitution Zr (Ti) for Mg will cause the lattice shrinkage or extension, resulting in the shift of the phonon frequency. At RT, the low frequency modes for doped ceramics in region "I" cannot be distinguished clearly, as compared to the pure ceramic. The intensity ratio of the modes located around 80 and 50 cm^{-1} is

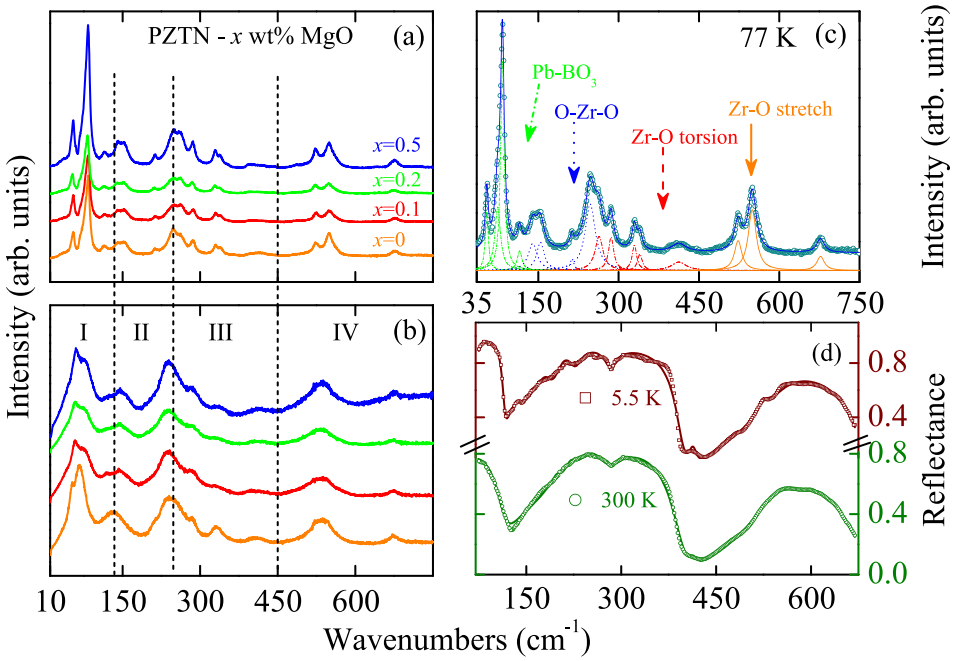

FIG. 1. Raman spectra of PZTN-x wt. % MgO ($x = 0$, 0.1, 0.2, and 0.5) ceramics recorded at (a) 77 K and (b) 300 K. (c) The multi-Lorentz peak fitting for pure PZTN at 77 K. (d) Experimental (dotted lines) and fitted (solid lines) infrared reflectance spectra at 5.5 and 300 K.

much smaller for doped ceramics, which can reflect the local symmetry divergence.

Fig. 1(d) shows the experimental and fitted FIR reflectance spectra of pure PZTN ceramic at 5.5 and 300 K, respectively. It indicates that temperature has obvious influence on the reflectance spectra. In order to extract the parameters of phonons that markedly contribute to the difference, the measured spectra can be fitted according to the expression:

$$R(\omega) = \left| \frac{\sqrt{\varepsilon(\omega)} - 1}{\sqrt{\varepsilon(\omega)} + 1} \right|^2, \tag{1}$$

where the dielectric function was represented by the dispersion formula of classical Lorentzian oscillators

$$\varepsilon(\omega) = \varepsilon_\infty + \sum_{k=1}^{n} \frac{S_k {\omega_k}^2}{{\omega_k}^2 - \omega^2 - i\omega\Gamma_k}. \tag{2}$$

Here, ε_∞, S_k, ω_k, Γ_k, and ω denote the permittivity due to high frequency electronic excitations, the phonon strength, eigenfrequencies, damping parameter of the kth phonon mode, and the frequency of the incident light, respectively. The best-fitting parameters for PZTN-x wt. % MgO ceramics at 5.5 and 300 K are listed in Table I. Note that nine oscillators were used to describe IR response and other allowed modes cannot be resolved due to small intensity or overlapping.

B. Lattice dynamics and dielectric functions

To study the evolution of lattice dynamics at low temperature region, the FIR reflectance at several temperatures for pure and 0.5 wt. % MgO doped PZTN ceramics is illustrated in Fig. 2. With increasing the temperature, striking variations can be observed around three regions as labeled by the arrows. The two dips located at 140 cm^{-1} are almost merged into one when the temperature rises up to 125 K. The variation may be due to the order-disorder process, which is related to the chain correlation length of the Pb^{2+} ion vibrations around the equilibrium positions. The disappearance of this mode can also be found in antiferroelectric $PbZrO_3$ ceramics.[28] While the peak around 410 cm^{-1} flattens progressively and disappears beyond 250 K. Similarly, the dip at 540 cm^{-1} becomes broadening and shifts to 560 cm^{-1} at 300 K for PZTN-0.5 wt. % MgO ceramic.

Fig. 3 depicts temperature dependent Raman spectra for MgO modified PZTN ceramics from 77 to 300 K. The peaks cannot be clearly distinguished at high temperature region. To get rid of the trivial temperature dependence, all Raman spectra have been divided by the Bose-Einstein occupation number $n(\omega) + 1 = 1/[1 - \exp(-\hbar\omega/k_B T)]$ ($\hbar$ and k_B are Planck constant and Boltzmann constant, respectively).[29] There exists a progressive change in frequency and broadening [full width at half maxima (FWHM)] of Raman modes. Most of peaks shift towards a lower wavenumber side due to reducing oscillator strength induced by thermal expansion. The peaks at 77 K correspond equivalently to the case of pure $PbZrO_3$, which demonstrates the antiferroelectric character of the structure.[30] The doubly splitting peaks around 330 and 530 cm^{-1} merged into single and broadening peak with increasing temperature. The high frequency mode (675 cm^{-1}) corresponds to the LO_4 branch, which shifts slightly with temperature and can be observed easily at low temperature.

Fig. 4 shows the dielectric functions (real part-permittivity ε' and imaginary part-loss ε'') derived from the simulation of FIR reflectance spectra. The dielectric loss spectra ε'' describe the polar-phonon absorption and the peaks correspond approximately to the transverse phonon eigenfrequencies. Fig. 4(c) presents difference spectra $\triangle\varepsilon'(T, w) = \varepsilon'(T, \omega) - \varepsilon'(5.5\ \mathrm{K}, \omega)$. It shows that the peak intensity and frequency change with temperature, especially below the 140 cm^{-1}. The region between 385 and 435 cm^{-1} is enlarged in the inset (d). It was observed that low frequency mode has the highest strength, which mainly contributes to the static dielectric constant. The dielectric constant from the optical

TABLE I. The parameter values of the classical Lorentz model for PZTN-x wt. % MgO ceramics are extracted from the best-fit FIR reflectance spectra at 5.5 and 300 K, respectively.

Sample	Temperature (K)	Parameter	ε_∞	E_1	E_2	E_3	E_4	E_5	E_6	E_7	E_8	E_9
$x=0$	5.5	S	6.84	66.7	2.44	7.45	10.7	4.48	0.95	0.05	0.51	1.64
		ω (cm^{-1})		76.9	136	179	205	233	288	412	523	544
		Γ (cm^{-1})		4.55	25.0	21.7	19.2	24.2	26.5	13.7	20.3	56.8
	300	S	4.50	65.5	…	4.32	5.37	2.98	1.18	0.02	1.45	0.06
		ω (cm^{-1})		61.5	…	199	216	236	286	413	526	583
		Γ (cm^{-1})		33.6	…	19.9	20.1	30.5	50.2	13.5	58.6	73.4
$x=0.1$	5.5	S	7.9	68.7	2.02	1.71	21.0	4.17	0.44	0.12	1.38	0.93
		ω (cm^{-1})		76.3	126	185	208	231	286	413	523	541
		Γ (cm^{-1})		7.43	32.1	11.6	10.7	16.4	12.7	25.0	18.1	21.1
	300	S	5.14	49.7	…	8.88	5.53	1.72	0.73	0.06	1.22	0.39
		ω (cm^{-1})		72.1	…	206	220	245	288	413	517	537
		Γ (cm^{-1})		28.2	…	15.1	17.2	30.5	36.1	24.1	37.2	31.7
$x=0.2$	5.5	S	6.87	59.9	1.83	3.38	14.2	4.35	0.80	0.06	1.04	1.06
		ω (cm^{-1})		77.5	139	182	207	236	288	412	523	544
		Γ (cm^{-1})		4.03	21.8	17.4	14.9	22.7	23.0	15.0	15.3	26.4
	300	S	5.56	48.4	…	8.62	6.14	2.16	1.23	0.06	1.69	0.08
		ω (cm^{-1})		72.1	…	206	220	245	288	413	517	537
		Γ (cm^{-1})		28.2	…	15.1	17.2	30.5	36.1	24.1	37.2	31.7
$x=0.5$	5.5	S	7.04	65.1	1.87	6.34	10.5	5.20	1.26	0.05	0.66	1.49
		ω (cm^{-1})		76.5	136	183	207	235	288	413	523	543
		Γ (cm^{-1})		5.77	22.7	20.4	18.5	25.6	30.9	14.3	16.0	41.6
	300	S	3.87	24.1	…	4.29	4.20	2.60	1.49	0.02	1.26	0.04
		ω (cm^{-1})		79.9	…	201	218	238	289	417	521	575
		Γ (cm^{-1})		25.4	…	19.1	20.2	31.3	58.7	16.1	56.6	33.1

contributions can be calculated as $\varepsilon(0) = \varepsilon_\infty + \sum_{k=1}^{n} S_k$.[31] With increasing MgO composition, the $\varepsilon(0)$ value at RT is 85.4, 73.4, 73.9, and 41.9, respectively. The reduction of dielectric constants can be due to the doubly ionized oxygen vacancies induced by Mg doping. Due to the lower valence of Mg^{2+}, the lack of position charge in the PZT system is compensated by oxygen vacancies. The Mg^{2+} dopants and oxygen vacancies form defect dipoles and stabilize the ferroelectric domain configuration.[32] It has also been reported that the oxygen vacancies are the most important conducting species in Mg and Nb doped PZT ceramics.[32] In addition, the decline of dielectric constants may be due to the density deterioration and smaller grain size, which imply more grain boundary and pinning effect of the domain wall.[33]

C. Order-disorder and antiferroelectric-ferroelectric phase transitions

The FIR data for the PZTN-x wt. % MgO ceramics reveal striking phonon-frequency anomalies in all

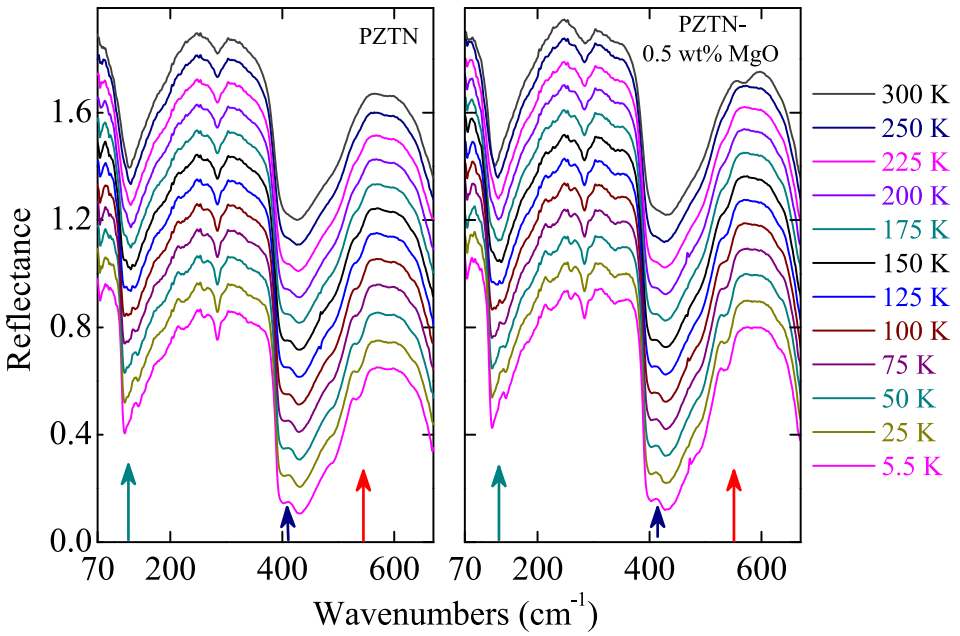

FIG. 2. Infrared reflectance spectra for PZTN-x wt. % MgO ($x=0$, 0.5) ceramics recorded at temperature from 5.5 to 300 K. The dramatic changes have been labeled by arrows around 140, 410, and 535 cm^{-1}. Each spectrum is shifted in the vertical direction for clarity.

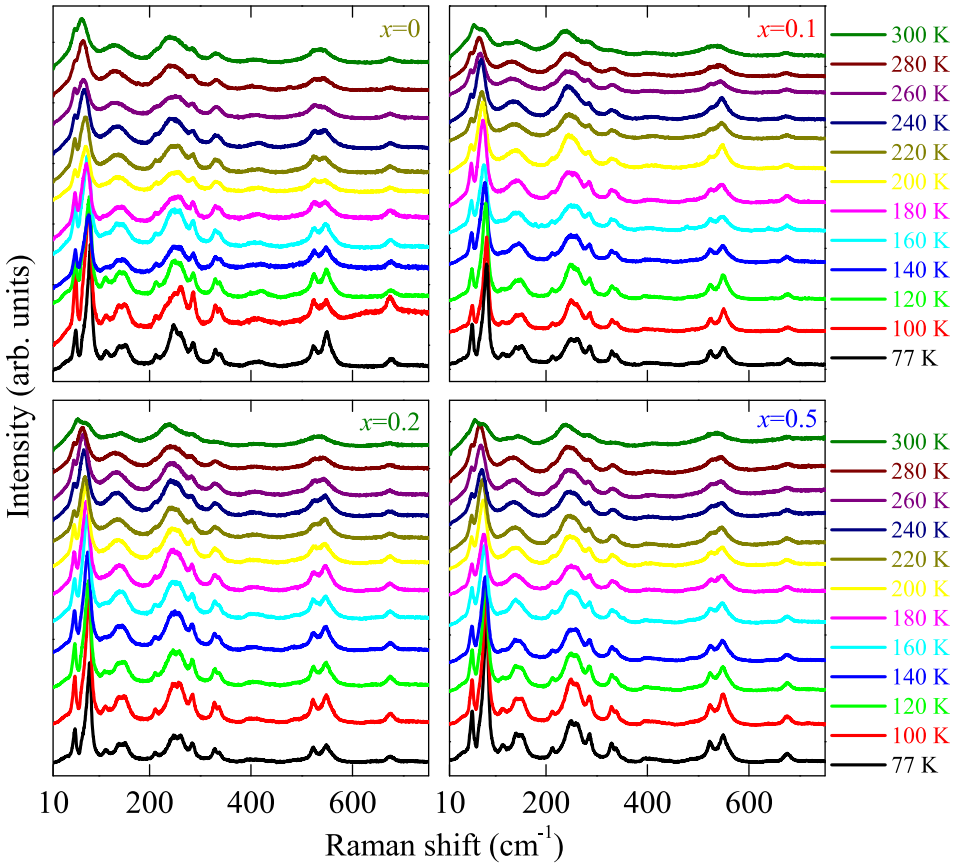

FIG. 3. Temperature-dependent Raman spectra for PZTN-x wt. % MgO ($x = 0$, 0.1, 0.2, and 0.5) from 77 to 300 K. Each spectrum is shifted in intensity for clarity.

compositions, as shown in Fig. 5. The change occurs near the phase transition temperature marked by the striations. The frequency of IR phonon modes shows similar red-shift trend with temperature due to lattice thermal expansion and anharmonic effects of lattice. The specific region around 120 K presents the high frequency phonon variation for pure PZTN ceramics. The mode located around 75 cm^{-1} can be assigned to soft E(TO1) mode, which corresponds to vibrations of Pb atom against the octahedra network perpendicular to the polarization.[20] The phonon of PZTN-x wt. % MgO ($x = 0.2$ and 0.5) around 540 and 75 cm^{-1} presents apparently steplike behavior near RT, confirming the changes of structure symmetry. The phase $F_{R(LT)}$ with space group $R3c$ is characterized by the tilting of oxygen octahedral about [111] direction with a consequent cell doubling (superstructure).[34] It indicates a phase transition of diffuse character towards low temperature ferroelectric state [AFE_{orth}–$F_{R(LT)}$](marked as T_{AFE}). Due to the diffuse character of the transition, the AFE-FE phase coexistence may occur in a wide temperature range. In comparison to pure and La-modified PZT 95/5 ceramics, the phase transition temperature decreases under the influence of Nb dopant.[35]

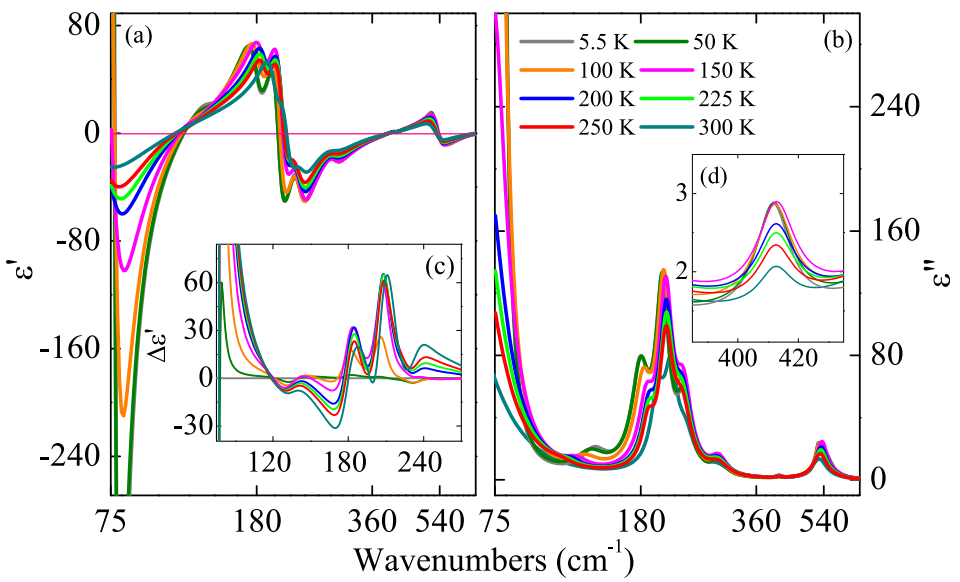

FIG. 4. (a) and (b) Spectra of complex dielectric functions $[\varepsilon(\omega) = \varepsilon' + i\varepsilon'']$ of pure PZTN at several temperatures. Inset (c) Difference spectra $\triangle\varepsilon'(T, \omega) = \varepsilon'(T, \omega) - \varepsilon'(5.5\,K, \omega)$; Inset (d) shows the enlarged imaginary part in the range of 385–435 cm^{-1}. The horizontal coordinate is the logarithmic unit to enlarge the low-frequency part.

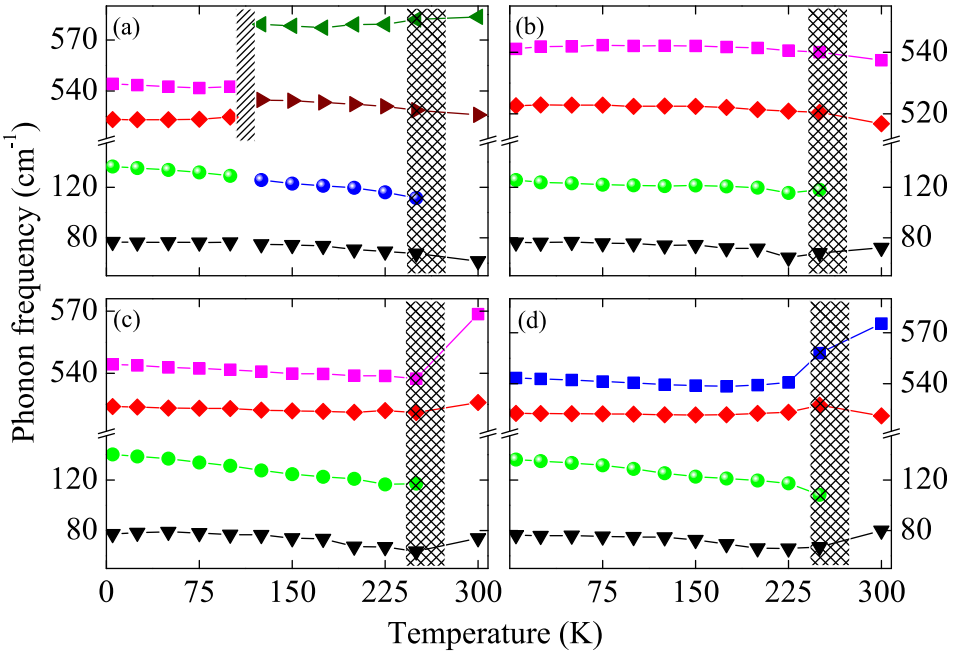

FIG. 5. Temperature dependence of IR-active phonon modes for PZTN-x wt. % MgO of (a) $x=0$, (b) $x=0.1$, (c) $x=0.2$, (d) $x=0.5$, respectively. Note that the shadow parts present the anomalies.

Fig. 6 presents the evolution of damping parameters and strength for the phonon modes from 5.5 to 300 K. Meanwhile, the phonon frequency of several Raman mode is depicted in Fig. 7. The damping is closely related to the anharmonicity, disordering of the structure, or enhancing of the local symmetry.[35] The dotted line indicates the second-type order-disorder transition (T_{OD}) near 120 K, beyond which the damping increases rapidly. The progressive evolution from an ordered phase to a partially disordered one is thermally activated and can be related to the disordered displacements of the atoms.[36] It is observed that the order-disorder transition temperature decreases slightly with increasing MgO composition, which may arise from the change of order degree due to the Mg substitution. The Mg doping effect is correlated with the movement of the ions (Zr, Ti, Nb, or Mg) in its oxygen octahedral. The mass, ionic radius, and valence of Mg^{2+}-dopant are responsible for the phase transition. Meanwhile, the Mg doping can break any correlation chains and create local permanent dipoles and influence the vibration strength.[35] The variation of Γ_{TO1} for the ceramics ($x=0.2$ and 0.5) around 250 K was sluggish, which was labeled by the striation. The damping of the phonon mode located at 75 cm^{-1} is described by the formula: $\Gamma(T)=\Gamma_1+\Gamma_0[1+2/(e^{\Theta/T}-1)]$, which takes the Bose-Einstein statistical factors into considerations. With increasing MgO composition, the value of Θ is estimated to 187,

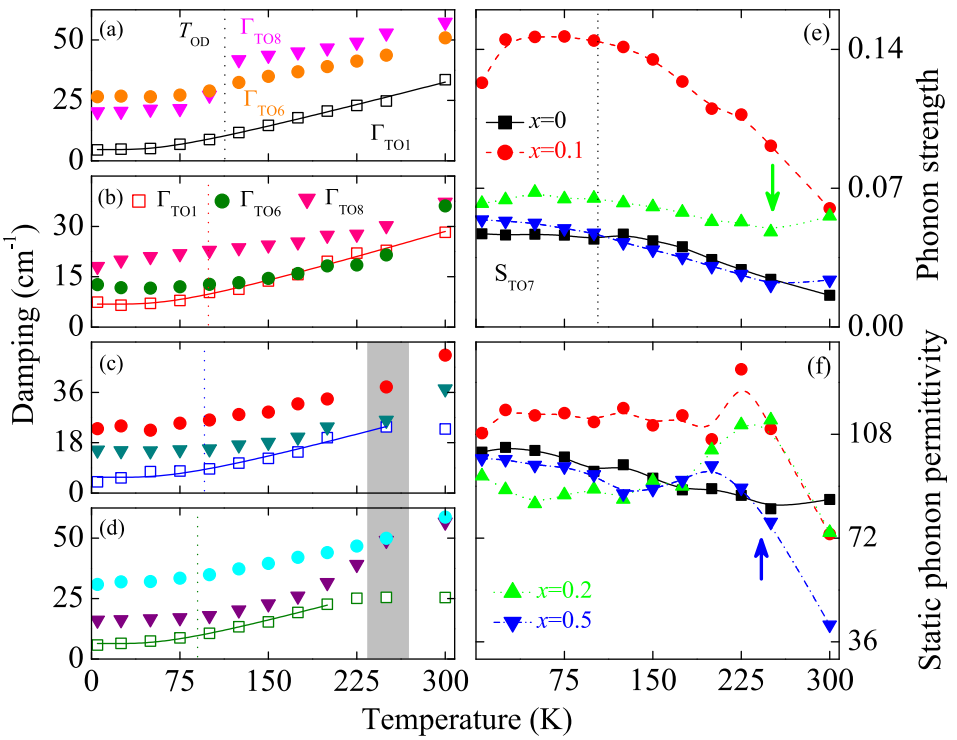

FIG. 6. (a)-(e) Temperature dependence of damping parameters (Γ_{TO1}, Γ_{TO6}, Γ_{TO8}) and phonon strength S_{TO7} for PZTN-x wt. % MgO ceramics ($x=0$, 0.1, 0.2, and 0.5). (f) Temperature dependence of the static phonon permittivity obtained from the sum of all phonon and electronic contributions (ε_∞). The dotted lines and striations (arrows) around 120 K and 250 K demonstrate the phase transitions T_{OD} and T_{AFE}, respectively.

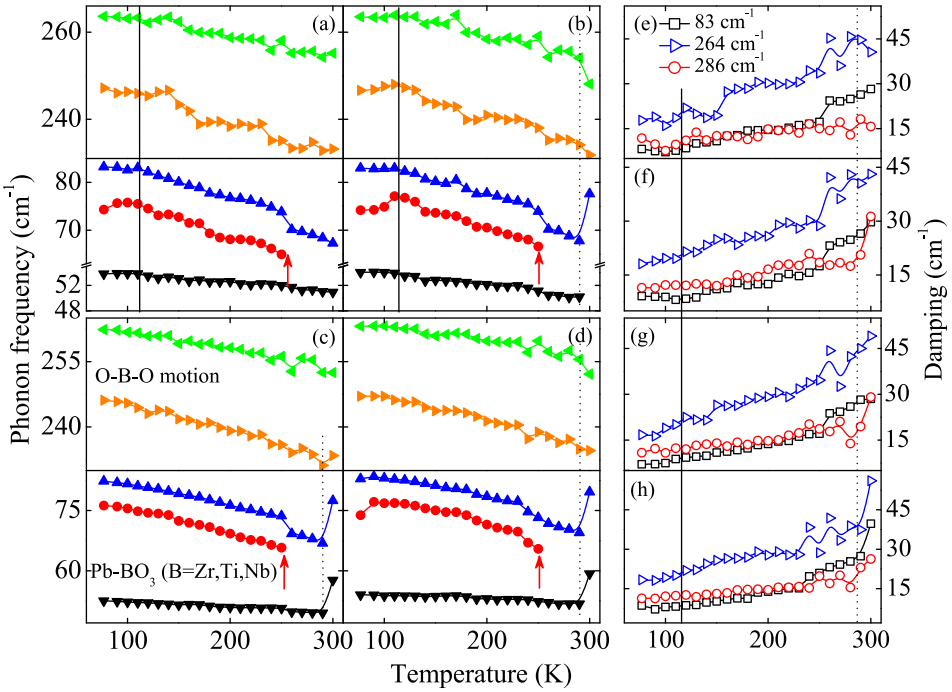

FIG. 7. Temperature dependence of phonon frequency and damping of several Raman active phonon modes for PZTN-x wt. % MgO ceramics of (a) and (e) $x=0$, (b) and (f) $x=0.1$, (c) and (g) $x=0.2$, (d) and (h) $x=0.5$, respectively. The arrows marked the transition temperature T_{AFE} around 250 K. The vertical dotted and solid lines labeled the transition from $F_{R(LT)}$ to $F_{R(HT)}$ and T_{OD}, respectively.

214, 225, and 202 K, respectively. It is higher than the Debye temperature (172 K) for pure PZT 95/5 ceramics, which is derived from the fitting of Einstein mode (38.1 cm^{-1}).[37]

Fig. 6(e) shows the strength variation from the phonon mode located around 410 cm^{-1}. It has slight variation between 5.5 K and T_{OD} and decreases sharply with increasing temperature. The behavior can also be observed from Fig. 4(d). This mode is related to the motion of B-site and oxygen atoms, which is sensitive to B-site arrangement and Mg^{2+} occupation. The specific region around T_{OD} can be attributed to the fluctuations of the order parameters and the long-range interactions make more contribution below the temperature. The oscillator strength of the mode shows sharp increase around the T_{AFE} for highly doped sample. The first-principle calculations on $PbZrO_3$ indicate that AFE displacements are associated with coupled rotations of the corner-connected oxygen octahedral ($\sum_3$ modes and R_{25}) and the Zr-O interaction plays an important role in the balance between short- and long-range forces.[18,38] The occurrence of AFE transition is due to the competition and cooperation among the modes instabilities. The behavior can also be found from the static phonon permittivity $\varepsilon(0)$ as a function of temperature in Fig. 6(f). It is derived from the sum of all phonon strength and electronic contributions and decreases sharply around T_{AFE} (labeled as arrows) for the doped PZTN ceramics.

Based on the fitting results, most of Raman active modes show similar behavior to that located around 264 cm^{-1}, as shown in Fig. 7. The frequency decreases with the temperature while the damping value increases. However, the mode located at 83 cm^{-1} shows some anomalous behavior. It has B_{1g} symmetry, which originates from the activation of low-frequency optic branch due to the folding at antiferrodistortive phase transition.[30] Thus, it is sensitive to the order-disorder mechanism and symmetry variation, which can reflect Pb-BO_3 lattice motion. Furthermore, Pb-O coupling is responsible for the involvement of Pb in ferroelectric soft mode eigenvector and the appearance of the antiferrodistortive instability in lattice dynamics of perovskites ABO_3.[28] As shown in Fig. 7, the frequency and broadening of the ceramics ($x=0$ and 0.1) keep almost unchanged below T_{OD}, and then varied linearly with increasing the temperature. The arrows marked the transition temperature T_{AFE} around 250 K. The AFE transformation involves the sluggish polar mode and nonpolar remaining ingredient. The former corresponds to the establishment of the AFE displacement of the Pb atom along ⟨110⟩ with a period of four pseudocubic unit cells, while the latter gives rise to the $a^-a^-c^0$ tilt pattern.[15] It also presents that the critical temperature T_{AFE} is weakly dependent on the MgO composition, which can be also found from IR active modes. The result is similar to that of Nb_2O_5 doped PZT 92/8, which derived from the measurement of dielectric constant and loss tangent.[39] The low-frequency modes present a sharp increment for the MgO-modified species, which is marked by the dotted lines. It can be related to the transition from $F_{R(LT)}$ to $F_{R(HT)}$. The transformation can be driven by the soft Γ_{25} oxygen rotational mode at the $q=(111)\pi/a$ or R point of the brillouin zone.[13,40] It arises from the shift of cation (Pb and Zr/Ti/Nb/Mg ions) along the ⟨111⟩ direction, which results from the coupling effect between oxygen's octahedra tilt and the spontaneous polarization.[41] The transition cannot be identified for pure PZTN ceramic with the present measurement, which suggests that the transition temperature is beyond room temperature. However, it is estimated to 290 K for MgO-doped PZTN ceramic and indicates that MgO dopant induces the shrinkage of transition temperature. The phenomenon can be due to the Mg^{2+} dopant, which results in the variation of cation shift and distortion of oxygen octahedra. With the aid of IR reflectance and Raman scattering, it is found that the MgO dopant has a remarkable effect on the lattice vibration and phase transition of PZTN ceramics.

IV. SUMMARY

To summarize, temperature and composition dependence of lattice dynamics and dielectric function in $Pb_{0.99}(Zr_{0.95}Ti_{0.05})_{0.98}Nb_{0.02}O_3$–$x$ wt. % MgO ($x = 0.0$, 0.1, 0.2, 0.5) ceramics have been investigated by FIR reflectance and Raman scattering below 300 K. Most of the phonon modes shows a red-shift trend with increasing the temperature due to lattice thermal expansion and anharmonic effects lattice. The static dielectric constant $\varepsilon(0)$ decreases with increasing MgO composition due to the existence of oxygen vacancies, which is typical characteristics for hard PZT. The features of phonon modes (frequency, broadening, and strength) present anomalies near the order-disorder transition, which slightly decreases with increasing MgO composition. Furthermore, the transition from antiferroelectric to low-temperature ferroelectric phase is observed near 250 K. It can be related to mode instability induced by the displacements and coupled rotations of the corner-connected oxygen octahedral. It indicates that Raman scattering and far-infrared reflectance are complementary and powerful tools to study lattice dynamics, which is sensitive to the structure and symmetry variation of perovskite oxides.

ACKNOWLEDGMENTS

This work was financially supported by Major State Basic Research Development Program of China (Grant Nos. 2011CB922200 and 2013CB922300), Natural Science Foundation of China (Grant Nos. 11374097 and 61376129), Projects of Science and Technology Commission of Shanghai Municipality (Grant Nos. 14XD1401500, 13JC1402100, and 13JC1404200), and the Program for Professor of Special Appointment (Eastern Scholar) at Shanghai Institutions of Higher Learning.

[1]B. Jaffe, W. R. Cook, and H. Jaffe, *Piezoelectric Ceramics* (Academic Press, London, 1971).
[2]D. I. Woodward, J. Knudsen, and I. M. Reaney, Phys. Rev. B **72**, 104110 (2005).
[3]M. Avdeev, J. D. Jorgensen, S. Short, G. A. Samara, E. L. Venturini, P. Yang, and B. Morosin, Phys. Rev. B **73**, 064105 (2006).
[4]Z. Ujma, J. Hańderek, and G. E. Kugel, Ferroelectrics **198**, 77 (1997).
[5]K. Leung, E. Cockayne, and A. F. Wright, Phys. Rev. B. **65**, 214111 (2002).
[6]D. A. Hall, J. D. S. Evans, S. J. Covey-Crump, R. F. Holloway, E. C. Oliver, T. Mori, and P. J. Withers, Acta Mater. **58**, 6584 (2010).
[7]G. A. Samara, Phys. Rev. Lett. **77**, 314 (1996).
[8]E. Buixaderas, I. Gregora, S. Kamba, P. Kužel, and I. Reaney, Appl. Phys. Lett. **94**, 052903 (2009).
[9]I. Grinberg, V. R. Cooper, and A. M. Rappe, Phys. Rev. B **69**, 144118 (2004).
[10]Z. Zhang, L. Li, C. Shu, and P. Wu, Appl. Phys. Lett. **89**, 152909 (2006).
[11]D. H. Zeuch, S. T. Montgomery, and J. D. Keck, J. Mater. Res. **7**, 3314 (1992).
[12]I. J. Fritz and J. D. Keck, J. Phys. Chem. Solids **39**, 1163 (1978).
[13]C. García, C. Aragó, and J. A. Gonzalo, Ferroelectrics **272**, 381 (2002).
[14]J. Hańderek and Z. Ujma, J. Phys.: Condens. Matter **7**, 1721 (1995).
[15]F. Cordero, F. Craciun, F. Trequattrini, C. Galassi, P. A. Thomas, D. S. Keeble, and A. M. Glazer, Phys. Rev. B **88**, 094107 (2013).
[16]K. Sanjoom and C. Puchmark, Ferroelectrics **416**, 47 (2011).
[17]B. Guiffard, E. Boucher, L. Eyraud, L. Lebrun, and D. Guyomar, J. Eur. Cera. Soc. **25**, 2487 (2005).
[18]Ph. Ghosez, E. Cockayne, U. V. Waghmare, and K. M. Rabe, Phys. Rev. B **60**, 836 (1999).
[19]W. J. Zhang, W. W. Li, X. G. Chen, Z. G. Hu, W. Liu, G. S. Wang, X. L. Dong, and J. H. Chu, Appl. Phys. Lett. **99**, 041902 (2011).
[20]E. Buixaderas, D. Nuzhnyy, J. Petzelt, L. Jin, and D. Damjanovic, Phy. Rev. B **84**, 184302 (2011).
[21]K. C. V. Lima, A. G. Souza Filho, A. P. Ayala, J. Mendes Filho, P. T. C. Freire, F. E. A. Melo, E. B. Araújo, and J. A. Eiras, Phys. Rev. B **63**, 184105 (2001).
[22]J. J. Zhu, K. Jiang, G. S. Xu, Z. G. Hu, Y. W. Li, Z. Q. Zhu, and J. H. Chu, J. Appl. Phys. **114**, 153508 (2013).
[23]S. Kamba, E. Buixaderas, J. Petzelt, J. Fousek, J. Nosek, and P. Bridenbaugh, J. Appl. Phys. **93**, 933 (2003).
[24]C. Carabatos-Nédelec, I. El Harrad, J. Handerek, F. Brehat, and B. Wyncke, Ferroelectrics **125**, 483 (1992).
[25]A. E. Pasto and R. A. Condrate, Sr., J. Am. Ceram. Soc. **56**, 436 (1973).
[26]D. W. Wang, E. Buixaderas, J. Íñiguez, J. Weerasinghe, H. Wang, and L. Bellaiche, Phys. Rev. Lett. **107**, 175502 (2011).
[27]R. D. Shannon, Acta Cryst. A **32**, 751 (1976).
[28]T. Ostapchuk, J. Petzelt, V. Zelezny, S. Kamba, V. Bovtun, V. Porokhonskyy, A. Pashkin, P. Kuzel, M. D. Glinchuk, I. P. Bykov, B. Gorshunov, and M. Dressel, J. Phys.: Condens. Matter **13**, 2677 (2001).
[29]A. Dubroka, J. Humlíček, M. V. Abrashev, Z. V. Popović, F. Sapiña, and A. Cantarero, Phys. Rev. B **73**, 224401 (2006).
[30]M. Hafid, G. E. Kugel, J. Handerek, and Z. Ujma, Ferroelectrics **135**, 101 (1992).
[31]R. P. S. M. Lobo, R. L. Moreira, D. Lebeugle, and D. Colson, Phys. Rev. B **76**, 172105 (2007).
[32]L. Eyraud, B. Guiffard, L. Lebrun, and D. Guyomar, Ferroelectrics **330**, 51 (2006).
[33]J. X. Wang, H. C. Nie, C. F. Lan, G. S. Wang, X. L. Dong, X. F. Chen, F. Cao, and H. L. He, Ceram. Int. **39**, 3915 (2013).
[34]H. Yi, M. G. Kim, J. H. Park, and H. M. Jang, J. Appl. Phys. **96**, 5110 (2004).
[35]I. EI-Harrad, P. Becker, C. Carabatos-Nédelec, J. Handerek, Z. Ujma, and D. Dmytrow, J. Appl. Phys. **78**, 5581 (1995).
[36]I. EI-Harrad, C. Carabatos-Nédelec, J. Handerek, Z. Ujma, and D. Dmytrow, J. Raman. Spec. **25**, 799 (1994).
[37]W. N. Lawless, Phys. Rev. B **14**, 134 (1976).
[38]A. G. Souza Filho, P. T. C. Freire, A. P. Ayala, J. M. Sasaki, I. Guedes, J. Mendes Filho, F. E. A. Melo, E. B. Araújo, and J. A. Eiras, J. Phys.: Condens. Matter **12**, 7295 (2000).
[39]Z. Ujma, L. Szymczak, J. Hańderek, K. Szot, and H. J. Penkalla, J. Eur. Ceram. Soc. **20**, 1003 (2000).
[40]Z. Xu, X. H. Dai, J. F. Li, and D. Viehland, Appl. Phys. Lett. **66**, 2963 (1995).
[41]N. Duan, N. Cereceda, B. Noheda, and J. A. Gonzalo, J. Appl. Phys. **82**, 779 (1997).